The pH-dependent Swelling of Weak Polyelectrolyte Hydrogels Modeled at Different Levels of Resolution

Jonas Landsgesell,[†] David Beyer,[†] Pascal Hebbeker,[‡] Peter Košovan,[*,‡] and Christian Holm[*,†]

[†]*Institute for Computational Physics, University of Stuttgart, D-70569 Stuttgart, Germany*

[‡]*Department of Physical and Macromolecular Chemistry, Charles University, Prague, Czechia*

E-mail: peter.kosovan@natur.cuni.cz; holm@icp.uni-stuttgart.de

[*]corresponding author

Abstract

The swelling of polyelectrolyte hydrogels has been often explained using simple models derived from the Flory-Rehner model. While these models qualitatively predict the experimentally observed trends, they also introduce strong approximations and neglect some important contributions. Consequently, they sometimes incorrectly ascribe the observed trends to contributions which are of minor importance under the given conditions. In this work, we investigate the swelling properties of weak (pH-responsive) polyelectrolyte gels at various pH and salt concentrations, using a hierarchy of models, gradually introducing various approximations. For the first time, we introduce a three-dimensional particle-based model which accounts for the topology of the hydrogel network, for electrostatic interactions between gel segments and small ions and for acid-base equilibrium coupled to the Donnan partitioning of small ions. This model is the

most accurate one, therefore, we use it as a reference when assessing the effect of various approximations. As the first approximation, we introduce the affine deformation, which allows us to replace the network of many chains by a single chain, while retaining the particle-based representation. In the next step, we use the mean-field approximation to replace particles by density fields, combining the Poisson-Boltzmann equation with elastic stretching of the chain. Finally, we introduce an ideal gel model by neglecting the electrostatics while retaining all other features of the previous model. Comparing predictions from all four models allows us to understand which contributions dominate at high or low pH or salt concentrations. We observe that the field-based models overestimate the ionization degree of the gel because they underestimate the electrostatic interactions. Nevertheless, a cancellation of effects on the electrostatic interactions and Donnan partitioning causes that both particle-based and field-based models consistently predict the swelling of the gels as a function of pH and salt concentration. Thus, we can conclude that any of the employed models can rationalize the known experimental trends in gel swelling, however, only the particle-based models fully account for the true effects causing these trends. The full understanding of differences between various models is important when interpreting experimental results in the framework of existing theories and for ascribing the observed trends to particular contributions, such as the Donnan partitioning of ions, osmotic pressure or electrostatic interactions.

1 Introduction

Polyelectrolyte hydrogels are polymer networks composed of covalently or reversibly cross-linked polyelectrolytes. Their characteristic feature is the ability to swell and absorb huge amounts of water, many times exceeding the mass of the dry gel. This swelling is caused by a combined effect of the electrostatic repulsion of charged monomers and the osmotic pressure of their counterions. *Weak polyelectrolyte* hydrogels contain weakly acidic or weakly basic groups that can change their ionization degree upon a change in the solution pH, which in turn affects their swelling properties. In addition to that,

the degree of ionization of the weak polyelectrolyte hydrogel determines the Donnan potential that in turn determines the partitioning of small ions between the hydrogel and the supernatant solutions, resulting in a complicated feedback loop. A theoretical understanding of these complex effects is important for applications of polyelectrolyte hydrogels in hygiene products[1], sequestration of ions[2,3] or water desalination[4–8] at a specific pH and salt concentration of the supernatant solution. It is also important for the design of pH-responsive hydrogels for controlled encapsulation and release of drugs, in which a change in the pH is used to control the swelling of the gel.[9–13]

Models predicting the swelling of weak polyelectrolyte hydrogels as a function of pH range from very simple ones, used in phenomenological theories, up to detailed molecular models used in simulations. The simple thermodynamic models usually employ rather crude approximations, based on the previous success of related models, on the authors' intuition, or sometimes based on computational convenience. We discuss some of these approximations in the paragraphs below. The main purpose of introducing more sophisticated models was to avoid some of these approximations, that usually came at the expense of increased computational cost. Therefore, the existing models dramatically differ not only in the employed approximations but also in computational requirements: the phenomenological equations can be solved analytically or numerically within seconds or minutes of computer time, whereas the simulation models typically require days or weeks of computer time to obtain the desired solution. Qualitatively, all the available models predict the key trends known from experiments on the swelling of polyelectrolyte hydrogels[14–16] and brushes:[17,18] (1) The gel swelling increases as the pH is increased; (2) The ionization of the gel, and concomitantly the gel swelling, is shifted towards pH values higher than the pK-value of the ionizable groups (assuming that the gel is a weak polyacid); (3) The gel swelling is non-monotonic as the salt concentration is increased, first increasing at low salt, then decreasing at high salt. Therefore, a natural question arises: What is the added value of complex simulation models, if they predict the same trends as the simple ones? The problem is that the success of various types of models has been assessed based on qualitative agreement with experimentally

observed trends, typically using different experimental data sets for different models. Because the experimental hydrogel samples are inherently imperfect, it is difficult to make a quantitative comparison of any model with experiments. Furthermore, a comparison with experiments makes it difficult to discern if the theoretical model ascribes the correct origin to a particular trend, or if the agreement in the predicted trends originates just by coincidence from a cancellation of errors, as has been witnessed many times in polymer science. In the current work, we avoid the uncertainty of comparing simulations with specific experiments by comparing the predictions of a set of models representing the same system at different levels of approximation. This approach allows us to critically evaluate the effect of each approximation on the predicted results, and to understand under which conditions this approximation is justified.

The simplest, and historically the oldest models of hydrogel swelling are based on expressions that approximate various contributions to the semi-grand potential Ω. They consider a two-phase system that consists of a gel phase coupled to an infinite reservoir of salt solution. Both these phases are assumed to be homogeneous but they have a different composition. The starting point of these models is the Flory-Rehner hypothesis,[19] stating that the semi-grand potential can be expressed as a sum of contributions originating from the chain stretching, the osmotic pressure of small ions, electrostatic interactions, and short-range interactions. In the case of weak polyelectrolyte gels, there is an additional contribution due to the acid-base equilibrium. The minimum of the semi-grand potential as a function of chain extension R_e then determines the swelling equilibrium. The relation between chain extension and gel volume is approximately described by an affine deformation of the network[20], such that

$$V_\mathrm{chain} = R_\mathrm{e}^3/A \tag{1}$$

where V_chain is the volume per chain and A is a geometrical prefactor that reflects the gel topology. Equivalently, the contributions to the semi-grand potential can be considered as contributions to the pressure acting on the gel, being the derivative of

free energy with respect to the volume, $P = -\partial\Omega/\partial V_{\text{chain}}$. The equilibrium is then attained at $P_{\text{ext}} = P^{\text{gel}} - P^{\text{res}} = 0$, where P_{ext} is the resultant external pressure applied on the gel, P^{gel} is the pressure inside the gel, and P^{res} is the pressure of the reservoir. It is important to point out that analogous models have been applied to the swelling of polyelectrolyte brushes, with the main difference being the geometry: the gels are assumed to swell uniformly in all three dimensions whereas the brushes swell just in one dimension.[21] In addition, interfacial effects in bulk gels can be neglected whereas the thickness of some brushes is not sufficient to neglect them. Similarly, interfacial effects need to be considered when modeling microgels. Therefore, brushes and microgels cannot be modeled as two-phase systems. Instead, their interface to the solution needs to be modeled explicitly.[22,23] Otherwise, the analogy between gels and brushes is very strong, so that all effects observed in gels can also be observed in brushes and vice versa.

In the ideal gas approximation, only the chain stretching and osmotic pressure of small ions are considered, whereas the contributions from electrostatic and short-range interactions are neglected. The stretching has been traditionally expressed by the harmonic approximation for a Gaussian chain. However, we have shown recently that this approximation is insufficient and should be replaced by a finite-extensible approximation, such as the Langevin function (see Eq. 23).[20,24,25] The osmotic pressure is given by the ideal-gas pressure of mobile ions in the gel and in the reservoir

$$P_{\text{osm}} = k_{\text{B}}T \sum_i (c_i^{\text{gel}} - c_i^{\text{res}}). \tag{2}$$

The concentration of mobile ions in the gel, and thereby also the osmotic pressure, is coupled to the concentration of charged groups in the gel by the Donnan equation that can be written as[26]

$$\frac{c_i^{\text{gel}}}{c_i^{\text{res}}} = \frac{z_i c_{\text{A}^-}}{2I^{\text{res}}} + \sqrt{\left(\frac{c_{\text{A}^-}}{2I^{\text{res}}}\right)^2 + 1}, \tag{3}$$

where c_i is the concentration of ions of type i with a valency q_i, and I^{res} is the ionic strength in the reservoir, $I^{\text{res}} = \frac{1}{2}\sum_i z_i^2 c_i^{\text{res}}$. For simplicity, in the following description

we assume that the gel is a weak polyacid, with c_{A^-} being the concentration of ionized acidic groups in the gel, that is coupled to pH in the gel by the Henderson-Hasselbalch equation,[27]

$$\mathrm{pH}^{\mathrm{gel}} - \mathrm{p}K = \log_{10}\left(\frac{\alpha}{1-\alpha}\right) \tag{4}$$

where pK is the acidity constant of the monomer and α is the ionization degree of the monomeric units of the gel. The acid-base equilibrium is also coupled to the Donnan partitioning of H^+ ions, resulting in different pH values inside and outside the gel

$$\mathrm{pH}^{\mathrm{res}} - \mathrm{pH}^{\mathrm{gel}} = \log_{10}(a^{\mathrm{gel}}_{\mathrm{H}^+}/a^{\mathrm{res}}_{\mathrm{H}^+}) \overset{\mathrm{ideal}}{=} \log_{10}(c^{\mathrm{gel}}_{\mathrm{H}^+}/c^{\mathrm{res}}_{\mathrm{H}^+}). \tag{5}$$

where a_{H^+} is the activity of H^+. The second equality in Eq. 5 is exact only for ideal systems. It is a good approximation, however, also for real systems because the deviations from the ideal behaviour in the gel and in the reservoir approximately cancel. Ultimately, the Donnan partitioning, gel swelling, and acid-base equilibrium are all mutually coupled, resulting in a system of non-linear equations that need to be solved iteratively even in the ideal case, *i.e.*, when all interactions are neglected. The ideal models described above can be extended to include short-range interactions approximated by the second and third virial coefficients,[28] or electrostatic interactions between the chain monomers using the Debye-Hückel theory,[29] while retaining the assumption of the gel phase being homogeneous.

Field-based models have been devised in order to account for the interactions and simultaneously avoid the assumption of a homogeneous gel phase. In the field-based models, inhomogeneous distributions of small ions and chain monomers are represented by spatially varying density fields, sometimes called density profiles. The semi-grand potential is then expressed as a functional of these fields. Then, the density profiles that minimize the semi-grand potential are found in a self-consistent iterative procedure. In this type of models, the electrostatic interactions are typically treated on the mean-field level, by using the Poisson-Boltzmann (PB) equation (see Eq. 18), coupled to the local acid-base equilibrium (see Eq. 20).[21,30–32] Furthermore, the mean-field models typically

employ another simplification that allows to reduce the three-dimensional problem to a one-dimensional one. To achieve this, they rely on the assumption of affine deformation, relating the end-to-end distance of the gel strands to the volume per chain in the gel. In some models of this class, the chains are represented as infinite rods, resulting in a cylindrically symmetric set-up. The density fields are then obtained by solving the PB equation in cylindrical symmetry, coupled to the chain stretching and acid-base equilibrium.[24] Others use the analogy with star polyelectrolytes, representing the gel as a network of stars, which results in a spherically symmetric problem and simultaneously allows to account for conformational flexibility of the polymer chains.[32] Analogous models have also been previously used for the modelling of pH-controlled ionization of star-like polyelectrolytes,[33] spherical and planar polyelectrolyte brushes.[30,31,34–36] While the assumption of affine deformation is well justified for polyelectrolyte brushes, its use for three-dimensional polyelectrolyte networks is more questionable.[20]

Particle-based simulation models can alleviate the main approximations used in the field-based models by explicitly accounting for pairwise interactions between particles and by sampling the configuration space using molecular simulations. For this purpose, coarse-grained (CG) models are most suitable, in which the particles represent one monomeric unit of the polymer or one ion in the solution, whereas the solvent is treated as a dielectric continuum. In principle, models with all-atom resolution could be used too, however, in practice they are computationally too demanding to probe the length- and time-scales relevant for polymer networks. The CG models can be constructed to represent a three-dimensional polymer network, thus alleviating the approximation of affine deformation,[20,37–43] or as single-chain models that rely on this approximation.[25] Furthermore, the CG models account for correlations between individual particles, going beyond the mean-field approximation. This is particularly important for electrostatic interactions that affect the pH-dependent ionization of weak polyelectrolyte gels. It has been shown for star-like polyelectrolytes that the mean-field approximation tends to underestimate the effect of interactions along the chain, especially with the nearest monomers,[33] and a similar effect can be expected for weak

polyelectrolyte hydrogels. CG models have not been previously employed for modelling of weak polyelectrolyte hydrogels, with the exception of a hybrid model that combined particle-based simulations with mean-field calculations of the ionization degree.[44–47] The CG models of our current study have been used before to model strong polyelectrolyte hydrogels with fixed ionization.[20,24,25] To study weak polyelectrolyte hydrogels, we now combine these models with the grand-reaction Monte Carlo (G-RxMC) method, which we introduced a year ago,[27] Thus, our current study for the first time combines a particle-based model of a weak polyelectrolyte hydrogel with an explicit model of acid-base reactions coupled to a reservoir of ionic solution. This set-up enables the comparison of predictions of swelling and ionization properties of weak polyelectrolyte hydrogels on different levels of approximation, starting from the ideal gas, through the mean-field, up to an explicit-particle representation.

Our article is structured as follows: we first introduce a hierarchy of particle-based and field-based models for polyelectrolyte hydrogels, which can be seen as a set of successive approximations. At the most detailed level, we introduce a coarse-grained particle-based, three-dimensional periodic gel model (gel MD), solved by molecular dynamics simulations in combination with the G-RxMC method. This model serves as a reference to which the simplified models are compared. As the first approximation, we introduce a cell gel model (CGM) which uses a particle-based description of a single polymer chain under tension in a square cuboid periodic box (chain MD). For the next level we replace the particle-based representation by a field-based one, representing the polymer chain as a charged cylinder under an elastic tension and accounting for electrostatic interactions by means of the Poisson-Boltzmann equation solved within a cylindrical cell, coupled to Donnan partitioning and acid-base equilibrium (PB CGM). Finally, we construct an ideal model as a modification of the PB CGM by disregarding the electrostatic interactions, while still retaining the coupling to Donnan and acid-base equilibrium (ideal CGM). By comparing the predictions obtained using this set of models, we are able to assess the impact of individual approximations on the final result.

2 Models of weak polyelectrolyte hydrogels

The real system that we would like to model consists of a weak polyelectrolyte hydrogel, i.e. a network of polyelectrolyte chains with pH-dependent ionization states, coupled to a buffer solution (reservoir) at a given pH and ionic strength. The gel structure is characterized by the chain length, $N = 40$, i.e. the number of monomeric units (segments) connecting two nodes of the network. The value of N was chosen as a typical value found for weak polyelectrolyte gels studied in various experimental works.[4,14,16,29,48] When specifically considering poly(acrylic acid) crosslinked by NN'-methylenebis(acrylamide), our chain length corresponds to 1.25 mol% of crosslinker, similar to the value used by Philippova *et al.*[14] Acid-base properties of the monomeric units of the network are characterized by the acidity constant $\mathrm{p}K = 4.0$, assuming that all of them are ionizable. The value of $\mathrm{p}K$ was chosen to be close to that of poly(acrylic acid), which is the most commonly used weak polyelectrolyte. The reservoir is characterized by its pH value and salt concentration. For simplicity, we assume that the reservoir contains only Na^+, Cl^-, H^+ and OH^- ions, which corresponds to a solution prepared by dissolving NaCl at a given concentration and subsequently adjusting the pH to the desired value by adding extra HCl or NaOH. We assume that the permittivity of the solvent corresponds to water at ambient temperature ($\varepsilon_r \approx 78$ at 25 °C). The permittivity and temperature fix the Bjerrum length to $\lambda_\mathrm{B} = e^2/4\pi\epsilon k_\mathrm{B}T \approx 0.71\,\mathrm{nm}$, which defines the length scale on which the interaction energy between two elementary charges is equal to the thermal energy, $k_\mathrm{B}T$. Furthermore, we assume that the reservoir is large enough such that its properties are not affected by the presence of the gel.

To represent the system described above, we designed two coarse-grained particle-based models, and two field-based models. The particle-based models are derived from the well-established Kremer-Grest polymer model,[49] whereas the field-based models are derived from the well-established Poisson-Boltzmann model of a rod-like polyelectrolyte chain[50], augmented by a tension term to account for the gel swelling.[24] In the particle-based models, the monomeric units and small ions are represented as spherical particles.

Their conformations in the configuration spaces are statistically sampled using molecular simulations and ensemble averages of the relevant observables are computed from these samples. The particle-based models explicitly account for correlations between various particles and for fluctuations in the observables. In the field-based models, we use a set of partial differential equations that relate the semi-grand potential of the system to the spatially varying density fields. The density fields determine the probability of finding a particle of a given type (monomeric unit of the polymer or a small ion) in a given region of space. The field-based models are solved using an iterative procedure, devised to obtain the density fields that correspond to the minimum of the semi-grand potential. Our field-based models thus account for interactions between the particles on the level of mean-field approximation and they do not account for fluctuations of the relevant observables. They account for correlations between various particles to a limited extent, within the mean-field approximation. As a limiting case of the PB field-based model, we introduce the ideal model that completely neglects the electrostatic interactions, however, it accounts for the Donnan partitioning, electroneutrality constraint and acid-base equilibrium. For brevity, we provide below just a simplified description of our models, focusing mainly on differences between them. The full technical details, including the values of all parameters, are provided in Ref.[62]

2.1 Particle-based models (MD)

In our particle-based models, each particle (monomeric unit or small ion) has the same effective size $\sigma = \lambda_B/2 = 0.355\,\mathrm{nm}$ that approximately corresponds to the size of monomeric unit of PAA, or to the effective size of solvated ions. We use the WCA potential[51] to account for steric repulsion, the FENE potential[52] to account for polymer connectivity and the Coulomb potential to account for electrostatic interactions. We use Langevin dynamics to simulate the evolution of the system in configuration space.

To account for the acid-base equilibrium and coupling to the reservoir, we use the grand-reaction Monte Carlo method, introduced in Ref.[27]. We represent the acid-base

ionization reaction as

$$\mathrm{HA} \rightleftharpoons \mathrm{A}^- + \mathrm{H}^+ \tag{6}$$

where A denotes a generic weak acid group, HA denotes its non-ionized form and A^- denotes its ionized form. The ionization reaction is modeled using the reaction ensemble formalism, a Monte-Carlo procedure, in which the identity of HA is changed to A^- and an H^+ is inserted into the system, based on the acceptance probabilities described in Refs.[27,53]. The system is coupled to a reservoir by inserting and deleting ion pairs, formally represented as chemical reactions

$$\emptyset \rightleftharpoons \mathrm{H}^+ + \mathrm{OH}^- \tag{7}$$

$$\emptyset \rightleftharpoons \mathrm{Na}^+ + \mathrm{Cl}^- \tag{8}$$

$$\emptyset \rightleftharpoons \mathrm{Na}^+ + \mathrm{OH}^- \tag{9}$$

$$\emptyset \rightleftharpoons \mathrm{H}^+ + \mathrm{Cl}^-. \tag{10}$$

where $\emptyset$ denotes an empty set. The equilibrium constants of these reactions are determined by the reservoir pH and salt concentration, as detailed in Refs.[27,62]. All particle-based simulations are performed using the simulation software ESPResSo.[54]

2.1.1 Periodic network gel model (gel MD)

Our three-dimensional (3D) periodic gel model is, up to parameter variations, the same model as described in earlier publications.[20,41,43] It consists of a perfect tetra-functional polymer network with diamond-like topology, as shown in Fig.1a. One unit cell in the cubic simulation box of length L contains $n = 16$ chains (gel strands) connected by eight nodes. To mimic the conditions of a macroscopic system, we use periodic boundary conditions (PBC).

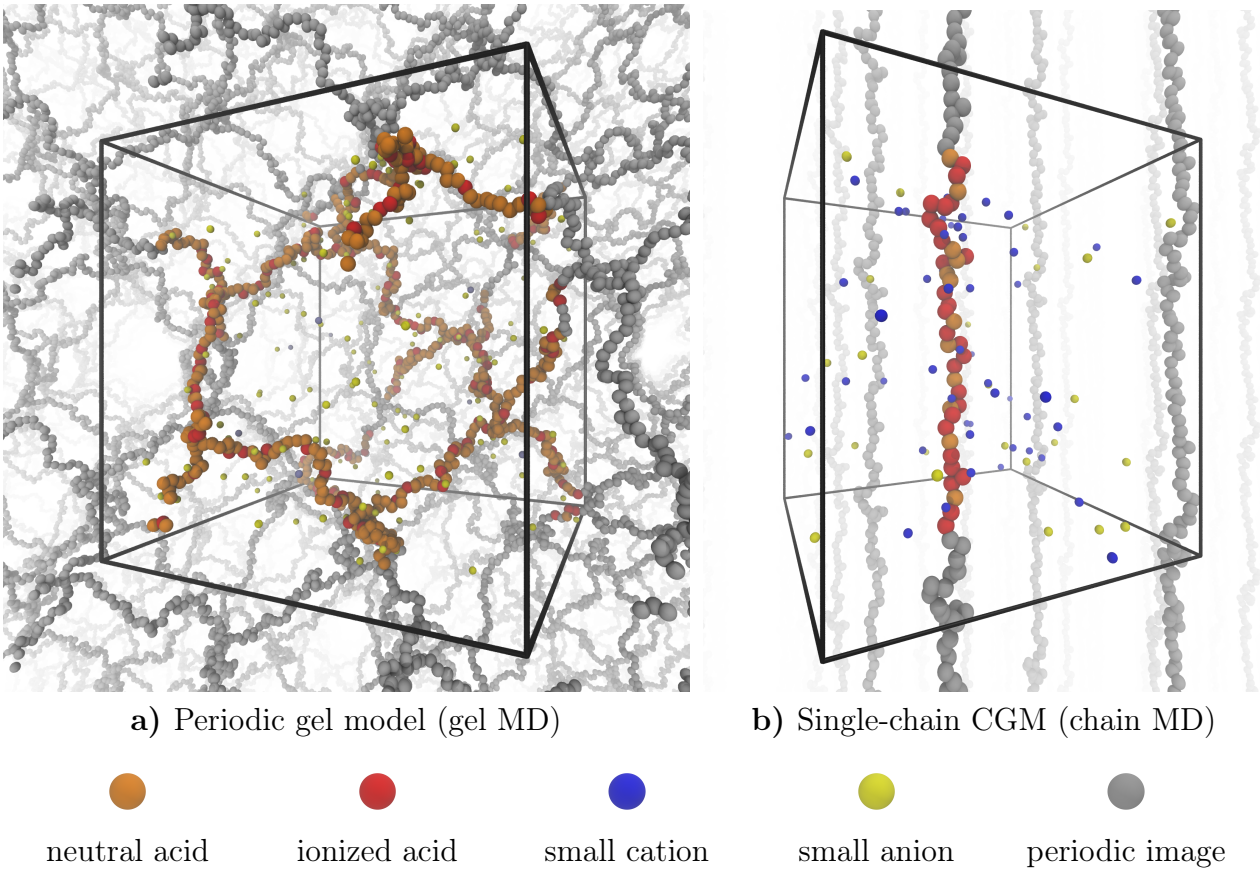

Figure 1: Schematic representation of the particle-based gel models used in the current study. The particle sizes are not shown to scale. The black box bounds the unit cell. Panel (a) shows the three-dimensional network gel model, i.e. a network of cross-linked polymer chains in a periodic cubic simulation box (gel MD); panel (b) shows the single-chain cell gel model (CGM) in a periodic square cuboid simulation box (chain MD)

The volume of the periodic gel is controlled by setting the box length, resulting in

$$V_{\text{chain}} = L^3/n \tag{11}$$

If the periodic gel is swollen so that the chains are fully stretched, then the volume per chain is given by Eq. 1 with the geometrical factor $A = \sqrt{27}/4$ that follows from the diamond topology.[20,43] If the periodic gel is not fully stretched, then Eq.1 is not exactly satisfied because positions of the network nodes can fluctuate.[20]

2.1.2 Single-chain cell gel model (chain MD)

The single-chain cell gel model (chain MD) uses a particle-based representation of a single chain, which is the first simplification of the periodic network gel model introduced in the previous section. By simulating just a single gel strand under tension, as shown in Fig.1b, we neglect the three-dimensional topology and many-body nature of the network but otherwise retain the full treatment of interactions and correlations between various types of particles within one chain. The single-chain CGM can thus be viewed as a mean-field attempt to factorize the many-body partition function of the macrogel into a product state of suitable identical subunits[55]. This simplification reduces the size of the simulated system by a factor of $n = 16$, thereby significantly reducing the computational cost.

To determine V_{chain} in the single-chain CGM, we assume that the gel deforms in an affine manner, so that Eq. 1 is valid at any swelling of the gel. We place the single chain in a square cuboid box of the same volume as given by Eq. 1, applying periodic boundary conditions in all directions, as shown in Fig.1b. We fix the end-to-end distance of the chain by connecting its first and last monomers by a bond through the periodic boundary conditions, and by fixing the x- and y-coordinates of these two particles. Then, by choosing the box length in the z-direction L_z, we set the end-to-end distance of the chain as

$$L_z = R_{\text{e}} + b \tag{12}$$

with the mean bond length $b \approx 0.966\sigma$. A posteriori, our results show that the mean bond length does not change significantly even at high stretching. Notably, this is true only if a sufficiently stiff FENE potential is used. If a harmonic potential is used to represent the bonds, then the mean bond length is significantly altered if the gel is highly stretched (swollen). The box length in the x and y directions, $L_{x,y}$, follows from the requirement that the total volume of the box is equal to the volume per chain

calculated from Eq. 1

$$V_{\text{chain}} = L_z^3/A = L_z \cdot L_{x,y}^2 \tag{13}$$

so that

$$L_{x,y} = L_z/\sqrt{A}. \tag{14}$$

It follows from Eq. 14 that the affine transformation results in a constant aspect ratio of the square cuboid box, $\alpha = L_{x,y}/L_z = 1/\sqrt{A}$, independent of chain stretching.

The use of a square cuboid box and periodic boundary conditions in the x- and y-direction allows the single chain to significantly overlap and interact with its periodic images at small end-to-end distances, thus mimicking the conditions in the three-dimensional periodic gel, where each strand interacts with other strands. This approach is different from our previous particle-based single-chain CGM[24,25] where the chain was placed inside a cylindrical cell with hard wall interactions in radial direction and periodicity in z-direction. We observed that interaction between the chain and the cylinder wall could lead to unphysical artefacts. At low chain extensions those were removed by using a square cuboid box with PBC. In addition, the square cuboid box allows us to directly employ the volume averaged isotropic virial pressure, avoiding the more complicated calculation of pressure in the cylinder that had to be performed in the previous studies.[24,25]

2.2 Field-based models

The following two models are field-based, considering spatially varying density profiles (fields) of each type of particles, instead of explicitly considering particle positions and pairwise interactions. These field-based models also consider only a single chain (gel strand) within a cylindrical cell under tension, and they assume an affine deformation of the network, which allowed us to relate the dimensions of the simulation box to the

volume per chain in the gel. Unlike the particle-based models, the field-based models are not solved by ensemble-averaging over simulation trajectories. Instead, they employ a set of partial differential equations that are solved iteratively, yielding the density profiles that correspond to minimum of the semi-grand potential. Therefore, these models neglect instantaneous fluctuations in particle densities, and they neglect also semi-grand potential contributions that originate from these fluctuations. Our two field-based models differ in how they treat electrostatic interactions. The PB cell gel model explicitly accounts for electrostatic interactions on the mean-field level by solving the PB equation. In addition to that, it also accounts for electroneutrality in the system and Donnan partitioning of small ions between the system and the reservoir. The acid-base equilibrium is taken into account by applying the Henderson-Hasselbalch equation to the local densities of the relevant particles. The other CGM neglects electrostatic interactions, considering only the Donnan partitioning and Henderson-Hasselbalch equation. Therefore, we refer to it as the ideal CGM.

2.2.1 Poisson-Boltzmann cell gel model (PB CGM)

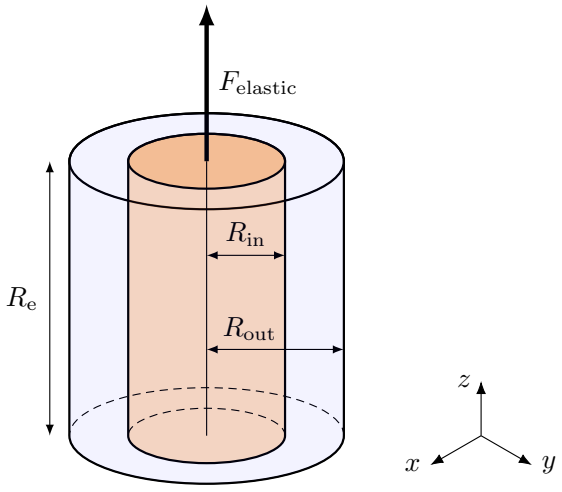

Figure 2: Schematic representation of the Poisson-Boltzmann CGM. Charges on the polymer are distributed homogeneously in the inner cylinder of radius R_{in}. The outer cylinder of radius R_{out} determines the volume per chain inside the hydrogel network. Periodic boundary conditions are applied in the z-direction.

This Poisson-Boltzmann CGM, introduced in previous works,[24,25] uses a continuum based description based on the charge densities of the polymer and the small ions. It can be viewed as a second mean-field step from the particle-based single-chain CGM. The model considers a charged rod mimicking the polyelectrolyte chain which is confined to a cylindrical cell of length L_z and radius R_{out} with PBC in the z-direction, that is set under tension, as shown in Fig. 2. Only inhomogeneities in the direction perpendicular to the axis of the cylinder are considered explicitly, so that the three-dimensional problem reduces to a one-dimensional problem that depends only on the distance from the cylinder axis, ρ. As in the case of the particle-based single-chain CGM, we assume an affine transformation of the network and set the cylinder height to the value of $L_z = R_{\text{e}} + b$ that leads to the cylinder volume

$$V_{\text{cyl}} = \pi R_{\text{out}}^2 L_z = L_z^3/A = V_{\text{chain}} \tag{15}$$

The radius of the cylinder is then given by

$$R_{\text{out}} = L_z/\sqrt{\pi A}. \tag{16}$$

For simplicity, we assume that chain monomers are homogeneously distributed inside an inner cylinder of radius R_{in}, so that the concentration of monomers at a distance $\rho = \sqrt{x^2 + y^2}$ from the cylinder axis is

$$c(\rho) = \theta\left(R_{\text{in}} - \rho\right) \frac{N}{\pi R_{\text{in}}^2 L_z} \tag{17}$$

where θ is the Heaviside step function. We fix the inner cylinder radius R_{in} by matching the radii of gyration in the x-y-plane of the cylindrical distribution and of a stretched chain in the direction perpendicular to the stretching force (see Ref.[62] for details).

To obtain the density profiles of small ions, we use the Poisson-Boltzmann equation with spatially varying electrostatic potential ψ. In the examined cylindrical geometry,

the symmetries lead to a one-dimensional problem in the variable $\rho \in [0, R_{\text{out}}]$:

$$\left(\partial_\rho^2 + \frac{1}{\rho}\partial_\rho\right)\psi(\rho) = -\frac{1}{\epsilon_\text{r}\epsilon_0}\left(q_+ c_+(\rho) + q_- c_-(\rho) + q_{\text{A}^-} c_{\text{A}^-}(\rho)\right). \tag{18}$$

Here, $c_{\text{A}^-}(\rho) = \alpha c(\rho)$ is the concentration of ionized monomers of the gel at the ionization degree α, that is constant inside the cylinder. The symbols c_+ and c_- refer to the concentrations of mobile cations and anions, which follow the Boltzmann distribution with respect to the electrostatic potential

$$c_i(\rho) = c_i^{\text{res}} \exp\left(-q_i\psi(\rho)/k_\text{B}T\right), \tag{19}$$

where c_i^{res} is the concentration of ion i in the reservoir. Because the whole cylinder has to be charge neutral, we impose the Neumann boundary condition $E_\rho(0) = E_\rho(R_{\text{out}}) = 0$, where $E_\rho \equiv -\partial_\rho\psi$. This boundary condition follows from Gauss's law and the imposed symmetries.

To determine $c_{\text{A}^-}(\rho)$, we use the charge regulation approach.[56,57] On the Poisson-Boltzmann level, the acid-base equilibrium can be expressed in terms of the local concentrations, which already reflect the excess contribution due to interactions of the mobile charged species with the electric field:

$$K_\text{A} = \frac{c_{\text{H}^+}(\rho)c_{\text{A}^-}(\rho)}{c_{\text{HA}}(\rho)c^\ominus}. \tag{20}$$

Here, $c^\ominus = 1\,\text{M}$ is the reference concentration. The total concentration of chain monomers inside the inner cylinder is given by Eq. 17, independent of the ionization degree. This allows us to eliminate $c_{\text{HA}}(\rho)$ from Eq. 20 and solve for $c_{\text{A}^-}(\rho)$:

$$c_{\text{A}^-}(\rho) = \frac{c(\rho)Kc^\ominus}{c_{\text{H}^+}(\rho) + Kc^\ominus}. \tag{21}$$

Equations 18, 19 and 21 represent a set of coupled non-linear partial differential equations that are solved iteratively to obtain a self-consistent solution for $\psi(\rho)$, $c_{\text{A}^-}(\rho)$

and $c_i(\rho)$. For this purpose, we use the FEM-solver implemented in version 5.6 of the software package COMSOL Multiphysics®.

To predict the swelling of polyelectrolyte gels under given conditions, it is necessary to compute the pressure acting on the gel in order to obtain a given volume per chain. The pressure inside the cylinder is given by a contribution of the cylinder top P_{cap} and a contribution of the cylinder walls P_{side}:[24,25,58]

$$P^{\mathrm{gel}} = \frac{1}{3}P_{\mathrm{cap}} + \frac{2}{3}P_{\mathrm{side}}. \tag{22}$$

The terms which contribute to the pressure consist of the kinetic pressure (ideal gas term), the Maxwell pressure due to the electric field which is readily obtained via the trace of the Maxwell stress tensor[59] and terms accounting for deformation of the gel, yielding

$$\begin{aligned} P_{\mathrm{cap}} = {} & \underbrace{k_{\mathrm{B}}T\sum_i \langle c_i\rangle_z}_{\text{kinetic}} + \underbrace{\frac{\epsilon_0\epsilon_r}{2}\langle E_\rho^2\rangle_z}_{\text{Maxwell}} - \underbrace{\frac{k_{\mathrm{B}}T}{\pi R_{\mathrm{out}}^2 b}\mathcal{L}^{-1}\left(\frac{R_{\mathrm{e}}}{R_{\max}}\right)}_{\text{stretching}} \\ & + \underbrace{\frac{k_{\mathrm{B}}T}{\pi R_{\mathrm{out}}^2 b}\cdot\frac{\sqrt{\langle R_{\mathrm{e,free}}^2\rangle}^3}{R_{\mathrm{e}}^3}\mathcal{L}^{-1}\left(\frac{\sqrt{\langle R_{\mathrm{e,free}}^2\rangle}}{R_{\max}}\right)}_{\text{confinement}} \end{aligned} \tag{23}$$

$$P_{\mathrm{side}} = k_{\mathrm{B}}T\sum_i c_i\left(R_{\mathrm{out}}\right) \tag{24}$$

where $\langle ...\rangle_z$ is the average over the cylinder cap and $\mathcal{L}^{-1}$ is the inverse Langevin function. Note that the Maxwell pressure does not contribute to the pressure on the cylinder wall due to the imposed Neumann boundary condition. The Langevin function rather than the commonly employed Gaussian stretching approximation is used because of the high extension that the chains can reach at high ionization degrees.[20] A detailed discussion of the different contributions can be found in the Ref.[62] The pressure in the reservoir

is calculated from the concentrations in the reservoir using the ideal gas law

$$P^{\mathrm{res}} = k_{\mathrm{B}}T \sum_i c_i^{\mathrm{res}}. \tag{25}$$

2.2.2 Ideal cell gel model (ideal CGM)

The ideal CGM is implemented using the same approach as the PB CGM, in the limit of vanishing electrostatic interactions $\epsilon_{\mathrm{r}} \to \infty$. For numerical stability we set $\epsilon_{\mathrm{r}} = 10^4$, effectively suppressing all electrostatic interactions, yielding the ideal-gas limit and homogeneous density profiles inside the cylinder. Thus, our ideal CGM takes into account the chain stretching, entropy of confinement, the Donnan partitioning of ions, and acid-base equilibrium via the Henderson-Hasselbalch equation. Admittedly, one could construct an even simpler ideal gel model. However, for the purpose of comparison it is advantageous that our ideal CGM employs identical approximations to the stretching pressure and affine deformation as the PB CGM.

3 Results

3.1 Determination of the swelling equilibrium

To determine the volume of the gel at free swelling equilibrium, we employ a pressure-concentration protocol, similar to the one used in previous works.[20,24,25,32,43,60,61] We perform a set of simulations at various volumes of the gel, defined by the simulation box length (L in the gel MD, L_z in the other models), in order to obtain the pressure-volume curves. We locate the swelling equilibrium by fitting the curve with an empirical smooth function $f(x) = a + b/\tan(x - c)$ where a, b and c are fit parameters. The intersection of the fit function with $P^{\mathrm{gel}}(L) - P^{\mathrm{res}} = 0$ yields the volume per chain at the free swelling equilibrium, V_{eq}. To obtain the ionization degree and other observables at free swelling equilibrium, we use the simulation with the box size closest to the determined value of V_{eq}. Fig. 3 (left panel) shows that, as the pH in the reservoir is increased,

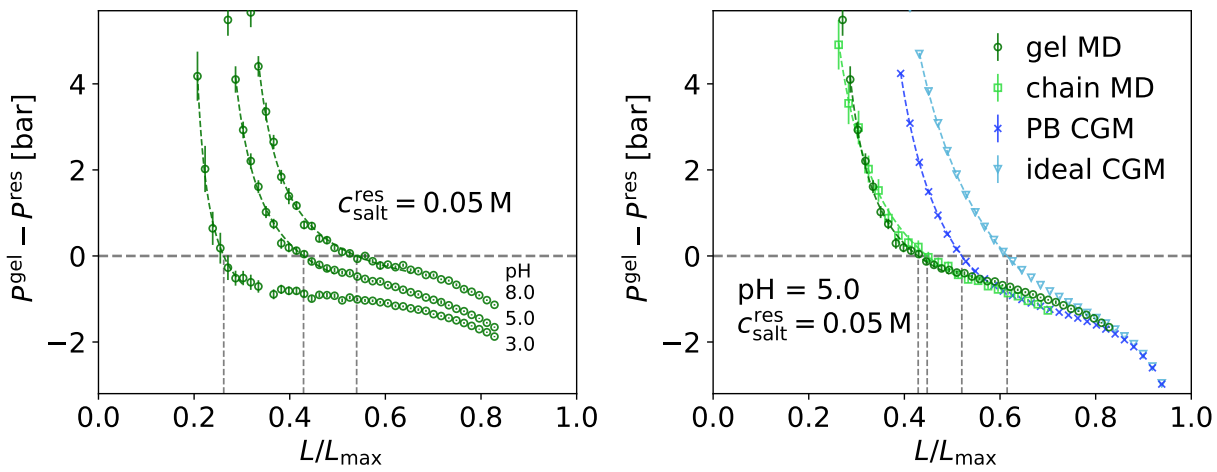

Figure 3: Pressure $P^{gel} - P^{res}$ as a function of simulation box length L for various models at selected conditions, as indicated in the figure. Left panel: simulation model of the periodic network gel model at one selected salt concentration and several pH values. Right panel: all models considered in this work at one selected value of pH and salt concentration. The dashed curves represent the fits which were used to determine the free swelling equilibrium. Vertical dashed lines represent the box length which corresponds to free swelling equilibrium. A full set of these curves for all simulated systems is provided in Ref.[62]

the intersection with $P = 0$ shifts to higher volumes, indicating an increased swelling of the gel as its ionization increases. Fig. 3 (right panel) shows that different models yield slightly different shapes of $P(L)$ curves, however, they follow the same general trend as a function of pH and added salt (see Ref.[62] for other values of pH and c_{salt}). In the following, we show how the ionization of the gel at free swelling equilibrium is related to the pH value in the reservoir, and how these two quantities determine the pH-dependent swelling of the gel.

3.2 pH-dependent ionization

Fig. 4(a,b) shows that the degree of ionization of the gel is shifted to higher pH values, as compared to the Henderson-Hasselbalch equation (HH, ideal titration curve). Equivalently, it can be viewed as if the ionization of the gel is suppressed when compared to the ideal ionization at a given pH. The shift of the curves decreases as the salt concentration in the reservoir increases (see also Ref.[62] for other salt concentrations).

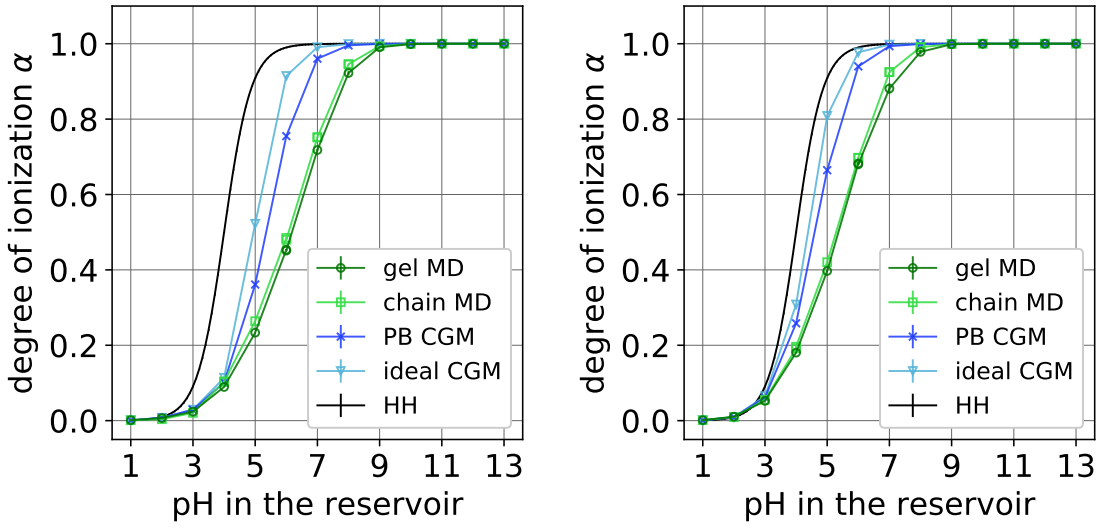

a) $\mathrm{pH}^{\mathrm{res}}$, $c_{\mathrm{salt}}^{\mathrm{res}} = 0.01\,\mathrm{mol/L}$ **b)** $\mathrm{pH}^{\mathrm{res}}$, $c_{\mathrm{salt}}^{\mathrm{res}} = 0.1\,\mathrm{mol/L}$

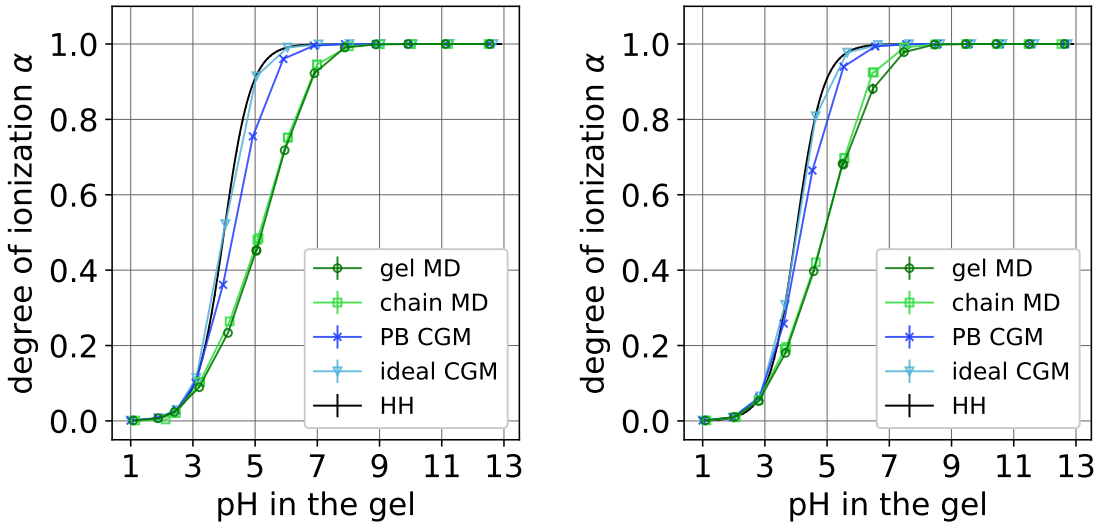

c) $\mathrm{pH}^{\mathrm{gel}}$, $c_{\mathrm{salt}}^{\mathrm{res}} = 0.01\,\mathrm{mol/L}$ **d)** $\mathrm{pH}^{\mathrm{gel}}$, $c_{\mathrm{salt}}^{\mathrm{res}} = 0.1\,\mathrm{mol/L}$

Figure 4: Degree of ionization as a function of pH *in the reservoir* (top row) and pH *in the gel* (bottom row) at low salt conditions ($c_{\mathrm{salt}} = 0.01\,\mathrm{M}$, left column) and high salt conditions ($c_{\mathrm{salt}} = 0.1\,\mathrm{M}$, right column).

Although these two general trends are well known from various experiments,[14,15] the variation of the ionization degree as a function of pH is not easy to measure directly. Therefore, it has been often inferred indirectly, typically from the variation of the gel swelling as a function of pH or from estimated values of the Donnan potential. These trends originate from two effects that have been termed the *Donnan effect*, caused by the Donnan partitioning of H^+ ions between the gel and the reservoir, and the *polyelectrolyte effect*, caused by direct electrostatic interactions between charged species (monomers and small ions).[26]

The well-known trends are qualitatively reproduced by all models, however, it is also clear that each model predicts a different deviation from the HH equation, increasing in the order ideal CGM < PB CGM < chain MD ≈ gel MD. For example, at low salt concentration $c_{\mathrm{salt}} = 0.01\,\mathrm{M}$ and pH = 5 the ideal curve predicts $\alpha \approx 1$, the ideal CGM predicts $\alpha \approx 0.5$ and the particle-based simulations both predict a very low ionization, $\alpha \approx 0.2$. The discrepancies in the predictions from the aforementioned models originate from the different treatment of electrostatic interactions. As a reference, we used the Henderson-Hasselbalch equation (HH) with pH in the reservoir as input. The ideal CGM model accounts for the Donnan effect within the ideal-gas approximation but completely neglects electrostatic interactions. Therefore, the ideal CGM curve is shifted to higher pH as compared the HH model, and this shift originates only from the Donnan partitioning of H^+ ions. The PB CGM accounts for Donnan partitioning and for electrostatic interactions on the mean-field level, which yields a lower bound to the exact result. Therefore, the shift predicted by the PB CGM is higher than from the ideal CGM. Finally, the two particle-based models (chain MD and gel MD) explicitly account for electrostatic interactions between individual charges and also for the Donnan partitioning. Consequently, both chain MD and gel MD models predict very similar shifts, which are greater than from the PB CGM. Furthermore, a comparison of Fig. 4a and Fig. 4b reveals that the ideal CGM and PB CGM capture about 50% of the full shift at low salt, whereas they capture a much smaller portion of the full shift at higher salt concentration. To understand the origin of these differences, it is

necessary to examine the Donnan and polyelectrolyte effects separately.

3.2.1 Effect of electrostatic interactions on the ionization

To demonstrate the role of the polyelectrolyte effect, in Fig.4(c,d) we plot α as a function of pH inside the gel, effectively subtracting the Donnan effect. The value of $\mathrm{pH}^{\mathrm{gel}}$ was calculated using Eq. 5 from the known $\mathrm{pH}^{\mathrm{res}}$ and concentrations of H^+ ions inside and outside the gel. As expected, Fig.4(c,d) shows that the ideal CGM result plotted as a function of $\mathrm{pH}^{\mathrm{gel}}$ coincides with the ideal HH result. Other models do not coincide with HH and the ideal CGM. Shifts in the ionization, predicted by these models, can be used as a measure of the polyelectrolyte effect on the ionization. Here, we observe that the PB CGM predicts a much smaller shift than the particle-based models, whereas the latter remain consistent with each other. The polyelectrolyte effect is only suppressed by an increase in the salt concentration, as evidenced by comparing $c_{\mathrm{salt}} = 0.01\,\mathrm{M}$ in Fig.4c and $c_{\mathrm{salt}} = 0.1\,\mathrm{M}$ in Fig.4d. This suppression can be attributed to the electrostatic screening, which affects mostly interactions among monomers that are separated by more than the Debye screening length (3 nm at $c_{\mathrm{salt}} = 0.01\,\mathrm{M}$ and 1 nm at $c_{\mathrm{salt}} = 0.1\,\mathrm{M}$). Notably, the polyelectrolyte effect is dominated by interactions between the nearest monomers, whereas the electrostatic screening affects mostly interactions between groups that are separated by 3-10 monomers along the chain. Therefore, in the relevant range of salt concentrations, the electrostatic screening only weakly affects the magnitude of the polyelectrolyte effect. However, Fig.4(c,d) clearly demonstrates that the approximation used for the electrostatic interactions is the key factor which determines the ability of a particular model to predict the polyelectrolyte effect.

3.2.2 pH in the gel due to Donnan partitioning

We quantify the Donnan effect by plotting the difference between the pH value in the gel and in the reservoir, $\mathrm{pH}^{\mathrm{gel}} - \mathrm{pH}^{\mathrm{res}}$, which is caused by the Donnan partitioning. Fig.5 shows that, at low salt $c_{\mathrm{salt}} = 0.01\,\mathrm{M}$, the Donnan effect can lead to a difference of about one unit of pH between the gel and the reservoir. This difference is small

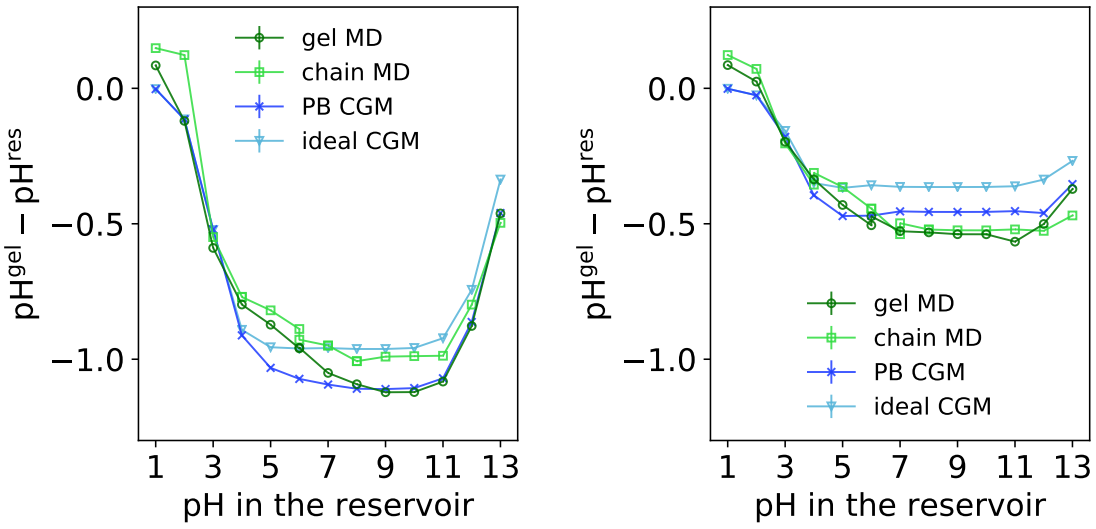

a) $\mathrm{pH}^{\mathrm{res}}$, $c_{\mathrm{salt}}^{\mathrm{res}} = 0.01\,\mathrm{mol/L}$ **b)** $\mathrm{pH}^{\mathrm{res}}$, $c_{\mathrm{salt}}^{\mathrm{res}} = 0.1\,\mathrm{mol/L}$

Figure 5: Difference between the pH values in the gel and in the bulk as a function of pH in the bulk at low concentration of added salt (left) and high concentration of added salt (right). The distinct curves were obtained using different models, as indicated in the legend.

at low pH, when the gel is non-ionized, however, it becomes significant at $\mathrm{pH} \gtrsim \mathrm{p}K$, as the gel ionization increases. The difference $\mathrm{pH}^{\mathrm{gel}} - \mathrm{pH}^{\mathrm{res}}$ is approximately constant at intermediate pH, $7 \lesssim \mathrm{pH}^{\mathrm{res}} \lesssim 11$, and it starts to diminish at $\mathrm{pH}^{\mathrm{res}} \gtrsim 12$. At high pH values the gel is fully ionized but the Donnan potential decreases as the ionic strength of the reservoir increases due to the additional NaOH, although the amount of added salt remains constant. At a higher salt concentration, $c_{\mathrm{salt}} = 0.1\,\mathrm{M}$, we observe the same dependence of $\mathrm{pH}^{\mathrm{gel}} - \mathrm{pH}^{\mathrm{res}}$ on pH, however, its magnitude is much smaller, accounting for less than 0.5 units of pH. Thus, the Donnan effect is strong at low salt concentration, and it becomes weak at a high salt concentration. By comparing the Donnan and the polyelectrolyte effects at various salt concentrations, we conclude that at low salt concentration the Donnan effect is comparable to the polyelectrolyte effect. At high salt concentration the Donnan effect almost vanishes and the shift of ionization is almost exclusively due to the polyelectrolyte effect. This observation is consistent with our previous study of weak polyelectrolyte solutions in equilibrium with a reservoir.[26]

Furthermore, Fig.5 shows that various models differ in predicting the magnitude of the Donnan effect, especially at pH values slightly above the pK. The field-based cell gel models, ideal CGM and PB CGM, predict a rather sharp onset of this effect within about 2 units of pH, reaching a saturation at pH $\approx 5 \approx$ p$K + 1$. In contrast, the particle-based models predict a more gradual onset of the Donnan effect, reaching a saturation value only at pH $\approx 8 \approx$ p$K + 4$. This difference is caused by coupling of the Donnan partitioning of ions and swelling of the gel, discussed in the next section.

3.3 Swelling of the gel

3.3.1 pH-dependent swelling

The swelling of polyelectrolyte gels is predominantly determined by the difference in osmotic pressures between the gel and the reservoir, and by the electrostatic interactions between the charged species. However, the osmotic pressure difference depends on the Donnan potential, which in turn depends on the ionization degree of the gel. The latter depends on pH in the gel, which in turn depends on the Donnan potential, resulting in a complicated feedback loop. In this section, we systematically investigate how this coupling affects predictions from various models of gel swelling.

To compare swelling properties of the hydrogels, we define the swelling ratio in two ways: (1) Based on the volume of the gel, $Q_{\mathrm{V}} = V/V_0$, which is directly proportional to the mass-based ratio used in experiments. Here, V_0 is the dry volume of the gel as estimated from a random packing of equally sized WCA-spheres (packing fraction approx. 64%); (2) Based on the end-to-end distance of the gel strands, $Q_{\mathrm{R_e}} = R_{\mathrm{e}}/R_{\mathrm{max}}$, assuming an affine deformation of the gel network upon swelling. In all models that assume an affine deformation, $Q_{\mathrm{V}} = Q_{\mathrm{R_e}}^3 \cdot V_{\mathrm{max}}/V_0$ where V_{max}/V_0 is constant, R_{e} is fixed, and the volume per chain can be calculated as $V = R_{\mathrm{e}}^3/A$. Only in the gel MD model, the chain ends are not fixed and their positions are allowed to fluctuate in all three dimensions. Therefore, Q_{V} and $Q_{\mathrm{R_e}}$ in the gel MD model are related in a more complicated way, reflecting the fact that the affine deformation is not strictly followed

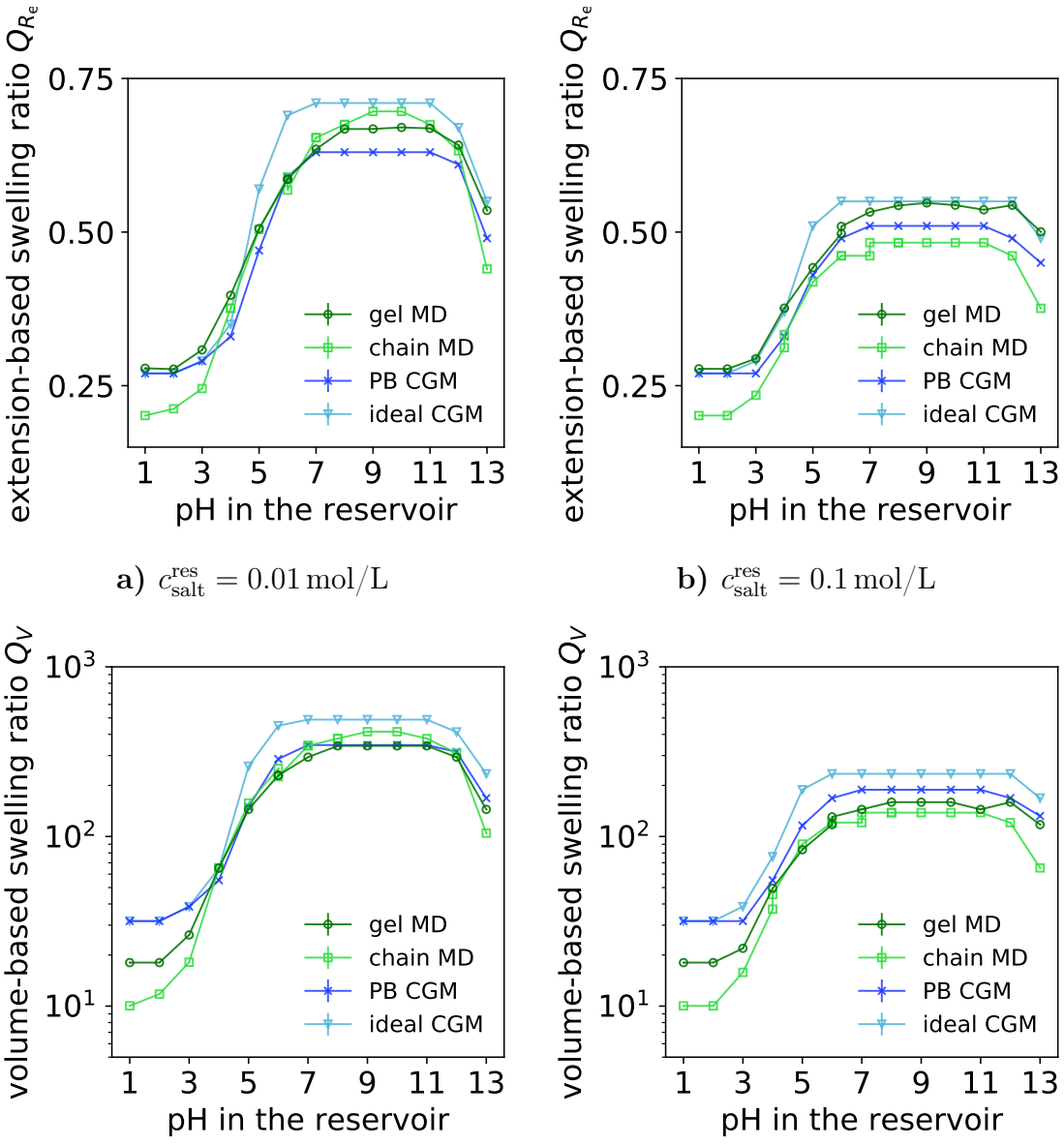

a) $c_{\text{salt}}^{\text{res}} = 0.01\,\text{mol/L}$ **b)** $c_{\text{salt}}^{\text{res}} = 0.1\,\text{mol/L}$

c) $c_{\text{salt}}^{\text{res}} = 0.01\,\text{mol/L}$ **d)** $c_{\text{salt}}^{\text{res}} = 0.1\,\text{mol/L}$

Figure 6: Swelling ratio of the gel as a function of the pH value in the reservoir expressed in terms of the chain extension $Q_{\text{R}_\text{e}} = R_\text{e}/R_{\text{max}}$ (top row) and in terms of the gel volume $Q_\text{V} = V/V_0$ (bottom row) at low concentration of added salt (left column) and high concentration of added salt (right column). The distinct curves were obtained using different models, as indicated in the legend.

upon gel swelling.[20]

Fig.6 shows that all models qualitatively capture the increase of swelling at pH $\approx$ pK and its decrease at a high pH. By comparing $Q_{\mathrm{R_e}}$ predicted by different models in Fig. 6 (a) and (b), we observe that both particle-based models agree almost quantitatively, except for the lowest pH values, where the gel is neutral. At low salt, the ideal CGM predicts an increase at pH $\approx$ pK that is steeper and occurs at lower pH values than in the simulations. In the saturation region at intermediate pH, the ideal CGM overshoots the maximum swelling. In contrast, the PB CGM predicts a lower swelling than the simulations at pH $\approx$ pK, although it predicts a higher ionization of the gel at the same pH values. Presumably, this seemingly contradicting observation is caused by a stronger Donnan partitioning in the PB CGM, as seen in Fig. 5. It affects both, ionization degree and swelling, however, because of the non-linear coupling, we observe a cancellation of errors in the mean-field approximation which predicts lower swelling despite higher ionization at the same pH values. The comparison of $Q_{\mathrm{R_e}}$ from different models at high salt yields a similar picture, except that the ideal CGM predicts a swelling closer to the gel MD model, whereas the chain MD model predicts a lower swelling than the gel MD model in the whole pH range.

Unlike $Q_{\mathrm{R_e}}$, a comparison of Q_{V} in Fig. 6 (c) and (d) displays a different picture than $Q_{\mathrm{R_e}}$. All models seem to disagree at low pH values, predicting a swelling in the order chain MD $<$ gel MD $<$ PB CGM $=$ ideal CGM. At intermediate and higher pH values, the chain MD and gel MD models agree at both, high and low salt conditions. The PB CGM agrees with both particle-based models at low salt whereas it predicts a higher swelling at low salt. Clearly, alleviating the assumption of affine deformation, as we have switched from $Q_{\mathrm{R_e}}$ to Q_{V}, has a notable impact on the comparison. This approximation has a particularly strong impact on the predicted swelling at low pH values and low degree of ionization, when the network is highly flexible and positions of the nodes can be far from their average positions on the diamond lattice, as evidenced by simulation snapshots in Fig. 7. In addition, the different treatment of excluded volume causes differences between the particle-based and the field-based models at low

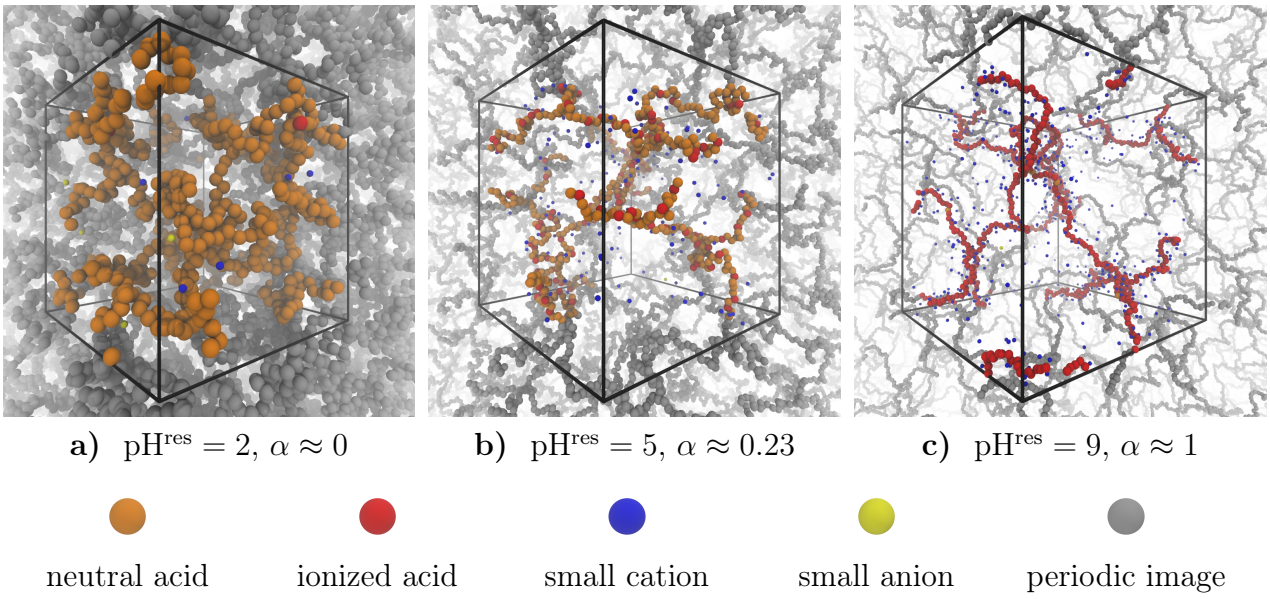

Figure 7: Snapshots of the gel MD model at free swelling equilibrium for a reservoir salt concentration of $c_{\text{salt}}^{\text{res}} = 0.01\,\text{M}$ and various pH values of the reservoir. The black box bounds the unit cell. The particles are not shown to scale.

pH values. At high pH, the structure of highly swollen gels is closer to the ideal diamond lattice, with the network nodes placed close to the actual location of lattice nodes. This is also supported by simulation snapshots in Fig. 7. Therefore, the relation $V = R_{\text{e}}^3/A$ is a good approximation at high swelling, whereas it fails at low swelling, as has been shown also in Ref.[20]. Then, the approximation for the electrostatic interactions is the key factor that determines the differences between the models. Consequently, both particle-based models predict the same Q_{V} at pH $\gtrsim$ pK, whereas the field-based models predict a higher swelling. Interestingly, all these differences cancel in the PB CGM at $c_{\text{salt}} = 0.01\,\text{M}$, where it predicts almost the same swelling as both particle-based models in the whole pH range, except at the lowest pH values.

3.3.2 Salt-dependent swelling

Finally, we investigate the mechanism of non-monotonic swelling as a function of added salt that has been observed in various experiments on polyelectrolyte hydrogels[14,15], polyelectrolyte brushes[21,31], and micelles.[17] For this purpose, we extended the range

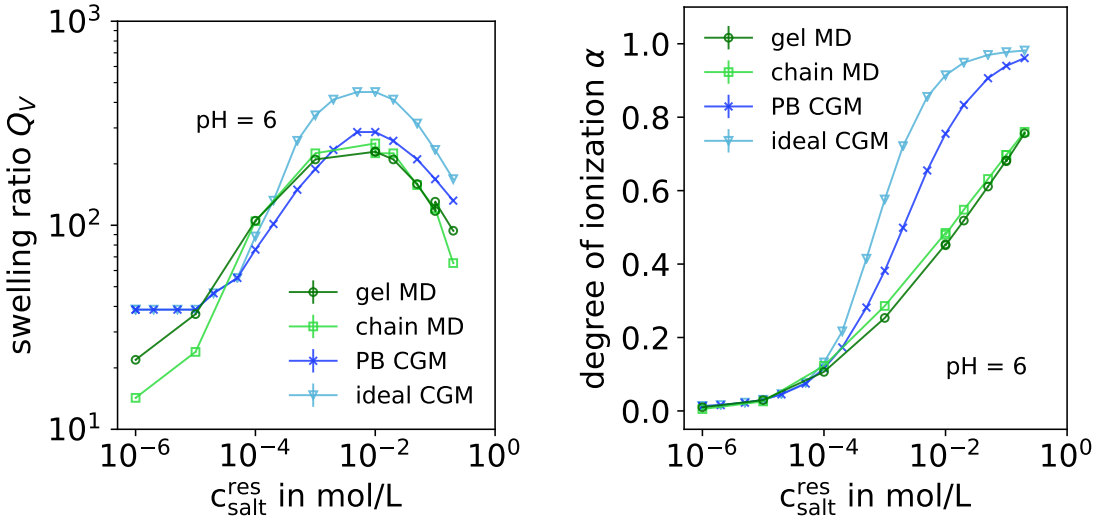

a) Volume-based swelling ratio **b)** Degree of ionization

Figure 8: The volume-based swelling ratio (top row) and the degree of ionization (bottom row), predicted from various models, as a function of added salt at pH = 6.

of investigated salt concentrations to very low values of c_{salt} at selected values of pH. In Fig.8(a,b) we show that, at pH = 6 $\gtrsim$ pK, the swelling first dramatically increases at low salt, $c_{\text{salt}} \lesssim 10^{-2}$ M, then it goes through a maximum and starts to decrease at $c_{\text{salt}} \gtrsim 10^{-1}$ M. All models predict a similar trend in the swelling as a function of salt concentration, except that the ideal CGM overshoots the maximum swelling, which was discussed already in the previous section. At pH = 8 $\gg$ pK, the swelling starts to increase at lower salt concentrations, followed by a broad maximum at intermediate salt concentrations, and eventually a decrease at high salt concentrations. On the contrary, both, swelling ratio and degree of ionization, are practically unaffected by the added salt at pH = 4 (see Ref.[62] for the corresponding figures).

Based on analytical theories and mean-field calculations, the following explanation of this phenomenon has been established:[21] as the salt concentration is increased, the Donnan potential decreases, resulting in an increasing ionization of the gel, which causes an increase in the swelling. Simultaneously, the increased salt concentration causes a decrease in the osmotic pressure, however, this decrease is overcome by the increasing ionization. The maximum swelling is reached when the gel becomes almost fully ion-

ized. From this point on, a further increase in salt concentration does not increase the ionization of the gel, instead, it decreases the osmotic pressure, causing a decrease in gel swelling. This explanation is qualitatively confirmed by our simulation results, as can be inferred by correlating the swelling ratios in Fig.8(a,b) and ionization degrees in Fig.8(c,d). At both pH values, the increase in swelling at low salt concentrations follows the trend of the increasing ionization degree, whereas at high salt concentrations the swelling decreases while the ionization degree is not affected.

Despite the qualitative agreement with the mean-field picture, our comparison reveals notable differences between the distinct models, which can be tracked down to the employed approximations. Let us first focus on pH $= 6 \gtrsim \mathrm{p}K$, comparing Fig. 8a and Fig. 8b. The ideal CGM that neglects electrostatic interactions, predicts a much steeper increase in the ionization, and a concomitant increase in swelling already at $c_{\mathrm{salt}} \approx 10^{-4}\,\mathrm{M}$. The PB CGM predicts an increase in ionization at about 10-times higher concentration than the ideal CGM, and concomitantly it also predicts an increase in the swelling at a higher salt concentration. The explicit-particle models predict a more gradual increase in the ionization, so that the full ionization is not reached even at $c_{\mathrm{salt}} \approx 1\,\mathrm{M}$. Interestingly, the gel swelling from particle-based models starts to increase at lower salt than from both, PB and ideal CGMs, and it reaches a maximum at $c_{\mathrm{salt}} \approx 10^{-3}\,\mathrm{M}$, when the ionization degree is only $\alpha \approx 0.3$. Both particle-based models predict that the swelling starts to decrease already at $c_{\mathrm{salt}} \approx 10^{-2}\,\mathrm{M}$, although the ionization degree is only $\alpha \approx 0.5$, and the latter continues to increase as the salt concentration is further increased. No such thing is observed in the ideal and PB CGMs, which predict that the maximum swelling occurs at $\alpha \gtrsim 0.8$. Thus, although all models predict the non-monotonic swelling as a function of added salt, they ascribe it to different effects. Thus, we observe that the explanation of the increase in swelling as a function of salt concentration changes qualitatively if electrostatic interactions are considered explicitly, instead of applying the mean-field approximation. The field-based models predict a much higher degree of ionization, thereby ascribing the swelling to a strong Donnan effect, while underestimating the role of electrostatic interactions. The

particle-based models predict a lower degree of ionization and concomitantly weaker Donnan effect. Nevertheless, the field-based models predict the same swelling as the particle-based models, which is a consequence of cancellation of errors caused by the approximate treatment of electrostatic interactions. On the contrary, the decrease in swelling at high salt is treated consistently in all models, irrespective of the approximation for the electrostatic interactions.

4 Conclusion

We introduced a hierarchy of models for weak polyelectrolyte hydrogels at different levels of approximation and computational complexity, which allowed us to study the swelling of these gel models as a function of salt and pH, and we could in detail investigate the coupling of the reservoir to the acid-base equilibria inside the gel and to the Donnan partitioning of small ions between the gels and the supernatant salt solution. On the most detailed level, we used a periodic network gel model (gel MD) which takes into account the acid-base ionization equilibrium and the exchange of small ions with a reservoir. This model employed the usual coarse-grained particle-based representation of a polyelectrolyte and small ions in implicit solvent, simulated using Langevin dynamics. The gel strands were connected to an infinite network with a diamond-like topology, similar to how strong polyelectrolyte gels have been simulated in previous works. In addition, our periodic network gel model included for the first time the acid-base reactions and exchange of ions with the reservoir by using the recently developed G-RxMC method. The periodic network gel model served as a reference for the more approximate models. As the first mean-field step, we reduced the network to a model of single chain in a cell under tension, termed the single-chain cell gel model (CGM). This gel strand was simulated in a square cuboid box under PBC and the gel swelling was calculated from the imposed chain extension by assuming an affine deformation. Otherwise, the chain MD model accounts for the acid-base equilibria, electrostatic interactions and partitioning of ions on the same level as the gel MD model. As a second mean-field

step, we replaced the particle-based representation of electrostatic interactions by a field-based one, representing the gel strand as a homogeneously charged cylinder under tension surrounded by a cloud of counterions. We calculated the distribution of counterions and ionization degree of the gel by solving the Poisson-Boltzmann (PB) equation coupled to the Donnan partitioning, therefore, we called this model PB CGM. Finally, we turned off the electrostatic interactions in the PB CGM to obtain an ideal CGM which neglects all interaction but still accounts for the gel connectivity, for the Donnan partitioning and for the acid-base equilibrium using the Henderson-Hasselbalch equation. A comparison of predictions obtained with these different models allowed us to assess the effect of various approximations on the obtained results.

All models qualitatively reproduced the known trends in ionization degree of the gel as a function of pH and salt concentration. The ionization degree of a polyelectrolyte gel is not easy to measure experimentally, however, these trends qualitatively follow from a common chemical knowledge. A quantitative comparison of the ionization degrees predicted by different models revealed significant differences between these predictions. The highest ionization at a given pH was predicted by the ideal CGM that neglects the direct electrostatic interactions but accounted for the Donnan effect on the ionization due to the partitioning of H^+ ions. The other models revealed that, in addition to the Donnan effect, the ionization is further suppressed due to electrostatic repulsion between charges on the polyelectrolyte chains, termed the polyelectrolyte effect. The PB CGM predicted a weaker polyelectrolyte effect than the two particle-based models (gel MD and chain MD), which included explicit electrostatic interactions between the particles. Our results have shown that the Donnan effect is strong at low salt concentrations and weak at high salt concentrations, as manifested by difference between the pH in the gel and in the reservoir. In contrast, the polyelectrolyte effect is only weakly affected by the salt concentration. Therefore, an approximate treatment or a complete neglect of the electrostatic interactions caused a significant under-estimation of the shift in the ionization degree, as compared to the Henderson-Hasselbalch equation.

All models qualitatively reproduced the known trends in gel swelling, caused by an

increase in ionization of the acid groups as a function of pH. As expected, the ideal CGM that predicted a higher ionization than the other models, predicted also a higher swelling at the same pH. However, the swelling predicted by the mean-field PB CGM was consistent with the two particle-based models (gel MD and chain MD), despite significant differences between the predicted ionization degrees as a function of pH. This unexpected agreement could be explained by a cancellation of errors in the mean-field treatment of electrostatics and Donnan partitioning. Additional inconsistencies in the predicted swelling, especially at very low degrees of ionization, could be tracked down to the assumption of the affine deformation, which was used in all models except the periodic network gel model.

The cancellation of effects in the ideal and mean-field models was most evident when comparing the predicted swelling and ionization degrees as a function of salt concentration at a fixed pH value. The non-monotonic swelling as a function of salt is caused by an interplay between the ionization, Donnan potential and osmotic pressure. The Donnan potential decreases as the salt concentration is increased, resulting in two effects with competing impact on gel swelling: (1) the ionization degree increases; (2) the osmotic pressure decreases. At low salt concentrations, the first effect dominates, resulting in an increasing swelling as a function of salt. At high concentrations, the second effect dominates, resulting in a decreasing swelling as a function of salt. Interestingly, all models consistently predict the increase and decrease in gel swelling as a function of salt. Although they all predict an increase in swelling at similar salt concentrations, they simultaneously predict an increase in ionization degree at salt concentrations which differ by an order of magnitude. These results demonstrate that the earlier success of field-based models in predicting the salt-dependent swelling of weak polyelectrolyte gels does not imply that these models correctly capture the key effects and that electrostatic interactions can be safely neglected. The particle-based models demonstrate that electrostatic interactions significantly affect the ionization degree of the gel, whereas their effect on gel swelling effectively cancels with other effects which contribute to the net result.

Finally, our comparison of models has shown that both, field-based and particle-based models, consistently predict the swelling of weak polyelectrolyte gels as a function of pH and salt concentration. However, they significantly differ in the predicting the ionization degree, which is one of the key aspects that determine the gel swelling. Thus, if one is interested only in the prediction of gel swelling, any of these models serves the purpose. In such a case, the choice of the model might be based on the computational demands, which significantly differ between the models. The ideal CGM and the PB CGM can be used almost interactively because they require seconds to minutes of computer time. In contrast, the particle-based models require typically days to months of computer time. However, their main advantage is that they also provide the correct prediction of ionization degree as a function of pH and salt concentration. Therefore, if a correct physical explanation of the observed effects is desired, the particle-based models should be used. Among the particle-based models, the computational cost of the single-chain CGM is lower by a factor of at least 16 as compared to the periodic network gel MD model, while their results are quantitatively consistent. They become inconsistent only at low ionization degrees of the gel because the affine deformation assumption is not accurate under these conditions. Thus, our study demonstrated convincingly the impact of various approximations on the predictions of swelling and ionization states of weak polyelectrolyte hydrogels as a function of pH and salt concentrations. This improved understanding can be used as a guidance to decide which approximation is suitable to describe a particular experimental system. And lastly, it will help to correctly explain experimental observations using predictions from various models.

5 Supporting Materials

Additional electronic supporting information, simulation data and scripts are available free of charge from Ref.[62].

6 Acknowledgments

PK acknowledges the financial support of the Czech Science foundation, grant 21-31978J. CH acknowledges funds by the German Research Foundation (DFG) – grants No. 451980436 and No. 268449726. Parts of this work were also performed within the collaborative framework of the research unit *Adaptive Polymer Gels with Controlled Network Structure (FOR2811)*, funded by the German Research Foundation under No. 423435431.

References

(1) Masuda, F. In *Superabsorbent Polymers Science and technology*, 1st ed.; Buchholz, F. L., Peppas, N. A., Eds.; ACS Symposium Series 573; American Chemical Society: Washington D.C., 1994; pp 88 – 98.

(2) Klaus Opwis, J. S. G., Thomas Mayer-Gall Recovery of Noble Metals by the Use of Functional Adsorber Textiles. *Tekstil* **2016**, *65*, 322–326.

(3) Pan, Y.; Liu, Z.; Wang, W.; Peng, C.; Shi, K.; Ji, X. Highly efficient macroporous adsorbents for toxic metal ions in water systems based on polyvinyl alcohol–formaldehyde sponges. *Journal of Materials Chemistry A* **2016**, *4*, 2537–2549.

(4) Höpfner, J.; Klein, C.; Wilhelm, M. A Novel Approach for the Desalination of Seawater by Means of Reusable Poly(acrylic acid) Hydrogels and Mechanical Force. *Macromolecular Rapid Communications* **2010**, *31*, 1337.

(5) Höpfner, J.; Richter, T.; Košovan, P.; Holm, C.; Wilhelm, M. In *Intelligent Hydrogels*; Sadowski, G., Richtering, W., Eds.; Progress in Colloid and Polymer Science; Springer International Publishing, 2013; Vol. 140; pp 247–263.

(6) Richter, T.; Landsgesell, J.; Košovan, P.; Holm, C. On the efficiency of a hydrogel-based desalination cycle. *Desalination* **2017**, *414*, 28–34.

(7) Arens, L.; Barther, D.; Landsgesell, J.; Holm, C.; Wilhelm, M. Poly(sodium acrylate) hydrogels: synthesis of various network architectures, local molecular dynamics, salt partitioning, desalination and simulation. *Soft Matter* **2019**, *15*, 9949–9964.

(8) Rud, O. V.; Landsgesell, J.; Holm, C.; Košovan, P. Modeling of weak polyelectrolyte hydrogels under compression, Implications for water desalination. *Desalination* **2021**, *506*, 114995.

(9) Oh, J. K.; Drumright, R.; Siegwart, D. J.; Matyjaszewski, K. The development of microgels/nanogels for drug delivery applications. *Progress in Polymer Science* **2008**, *33*, 448–477.

(10) Hamidi, M.; Azadi, A.; Rafiei, P. Hydrogel nanoparticles in drug delivery. *Advanced Drug Delivery Reviews* **2008**, *60*, 1638–1649.

(11) Makino, K.; Idenuma, R.; Murakami, T.; Ohshima, H. Design of a rate- and time-programming drug release device using a hydrogel: pulsatile drug release from kappa-carrageenan hydrogel device by surface erosion of the hydrogel. *Colloids and Surfaces B-Biointerfaces* **2001**, *20*, 355–359.

(12) Tada, D.; Tanabe, T.; Tachibana, A.; Yamauchi, K. Drug release from hydrogel containing albumin as crosslinker. *Journal of Bioscience and Bioengineering* **2005**, *100*, 551–555.

(13) Wang, Q.; Li, S.; Wang, Z.; Liu, H.; Li, C. Preparation and Characterization of a Positive Thermoresponsive Hydrogel for Drug Loading and Release. *Journal of Applied Polymer Science* **2009**, *111*, 1417–1425.

(14) Philippova, O. E.; Hourdet, D.; Audebert, R.; Khokhlov, A. R. pH-responsive gels of hydrophobically modified poly (acrylic acid). *Macromolecules* **1997**, *30*, 8278–8285.

(15) Ricka, J.; Tanaka, T. Swelling of ionic gels: quantitative performance of the Donnan theory. *Macromolecules* **1984**, *17*, 2916–2921.

(16) Tang, J.; Katashima, T.; Li, X.; Mitsukami, Y.; Yokoyama, Y.; Sakumichi, N.; Chung, U.-i.; Shibayama, M.; Sakai, T. Swelling Behaviors of Hydrogels with Alternating Neutral/Highly Charged Sequences. *Macromolecules* **2020**, *53*, 8244–8254.

(17) Matějicek, P.; Podhajecka, K.; Humpolicková, J.; Uhlik, F.; Jelinek, K.; Limpouchova, Z.; Prochazka, K.; Špirková, M. Polyelectrolyte behavior of polystyrene-block-poly (methacrylic acid) micelles in aqueous solutions at low ionic strength. *Macromolecules* **2004**, *37*, 10141–10154.

(18) Ferrand-Drake del Castillo, G.; Hailes, R. L. N.; Dahlin, A. Large Changes in Protonation of Weak Polyelectrolyte Brushes with Salt Concentration – Implication for Protein Immobilization. *The Journal of Physical Chemistry Letters* **2020**, *11*, 5212–5218.

(19) Flory, P. J.; John Rehner, J. Statistical Mechanics of Cross-Linked Polymer Networks II. Swelling. *The Journal of Chemical Physics* **1943**, *11*, 521–526.

(20) Košovan, P.; Richter, T.; Holm, C. Modeling of Polyelectrolyte Gels in Equilibrium with Salt Solutions. *Macromolecules* **2015**, *48*, 7698–7708.

(21) Borisov, O. V.; Zhulina, E. B.; Leermakers, F. A.; Ballauff, M.; Müller, A. H. E. In *Self Organized Nanostructures of Amphiphilic Block Copolymers I*; Müller, A. H. E., Borisov, O., Eds.; Adv. Polym. Sci.; Springer Berlin / Heidelberg, 2011; Vol. 241; pp 1–55.

(22) Hofzumahaus, C.; Hebbeker, P.; Schneider, S. Monte Carlo simulations of weak polyelectrolyte microgels: pH-dependence of conformation and ionization. *Soft Matter* **2018**, *14*, 4087–4100.

(23) Hofzumahaus, C.; Strauch, C.; Schneider, S. Monte Carlo simulations of weak polyampholyte microgels: pH-dependence of conformation and ionization. *Soft Matter* **2021**, 10.1039.D1SM00433F, tex.ids= hofzumahaus2021a.

(24) Landsgesell, J.; Sean, D.; Kreissl, P.; Szuttor, K.; Holm, C. Modeling Gel Swelling Equilibrium in the Mean Field: From Explicit to Poisson-Boltzmann Models. *Physical Review Letters* **2019**, *122*, 208002.

(25) Landsgesell, J.; Holm, C. Cell Model Approaches for Predicting the Swelling and Mechanical Properties of Polyelectrolyte Gels. *Macromolecules* **2019**, *52*, 9341–9353.

(26) Landsgesell, J. Simulation and Modeling of Polyelectrolyte Gels. Ph.D. thesis, 2020.

(27) Landsgesell, J.; Hebbeker, P.; Rud, O.; Lunkad, R.; Kosovan, P.; Holm, C. Grand-Reaction Method for Simulations of Ionization Equilibria Coupled to Ion Partitioning. *Macromolecules* **2020**, *53*, 3007–3020.

(28) Polotsky, A. A.; Plamper, F. A.; Borisov, O. V. Collapse-to-Swelling Transitions in pH- and Thermoresponsive Microgels in Aqueous Dispersions: The Thermodynamic Theory. *Macromolecules* **2013**, *46*, 8702–8709.

(29) Katchalsky, A.; Michaeli, I. Polyelectrolyte gels in salt solutions. *Journal of Polymer Science* **1955**, *15*, 69.

(30) Nap, R.; Gong, P.; Szleifer, I. Weak polyelectrolytes tethered to surfaces: Effect of geometry, acid-base equilibrium and electrical permittivity. *Journal of Polymer Science Part B: Polymer Physics* **2006**, *44*, 2638–2662.

(31) Klein Wolterink, J.; van Male, J.; Cohen Stuart, M. A.; Koopal, L. K.; Zhulina, E. B.; Borisov, O. V. Annealed Star-branched Polyelectrolytes in Solution. *Macromolecules* **2002**, *35*, 9176–9190.

(32) Rud, O.; Richter, T.; Borisov, O.; Holm, C.; Košovan, P. A self-consistent mean-field model for polyelectrolyte gels. *Soft Matter* **2017**, *13*, 3264–3274.

(33) Uhlík, F.; Košovan, P.; Limpouchová, Z.; Procházka, K.; Borisov, O. V.; Leermakers, F. A. M. Modeling of Ionization and Conformations of Starlike Weak Polyelectrolytes. *Macromolecules* **2014**, *47*, 4004–4016.

(34) Klein Wolterink, J.; van Male, J.; Daoud, M.; Borisov, O. V. Starburst polyelectrolytes: Scaling and self-consistent-field theory. *Macromolecules* **2003**, *36*, 6624–6631.

(35) Gong, P.; Genzer, J.; Szleifer, I. Phase Behavior and Charge Regulation of Weak Polyelectrolyte Grafted Layers. *Physical Review Letters* **2007**, *98*, 018302.

(36) Nap, R. J.; Tagliazucchi, M.; Szleifer, I. Born energy, acid-base equilibrium, structure and interactions of end-grafted weak polyelectrolyte layers. *The Journal of Chemical Physics* **2014**, *140*, 024910.

(37) Schneider, S.; Linse, P. Swelling of cross-linked polyelectrolyte gels. *European Physical Journal E* **2002**, *8*, 457–460.

(38) Yan, Q.; de Pablo, J. J. Monte Carlo Simulation of a Coarse-Grained Model of Polyelectrolyte Networks. *Physical Review Letters* **2003**, *91*, 018301.

(39) Edgecombe, S.; Schneider, S.; Linse, P. Monte Carlo Simulations of Defect-Free Cross-Linked Gels in the Presence of Salt. *Macromolecules* **2004**, *37*, 10089–10100.

(40) Yin, D.-W.; Yan, Q.; de Pablo, J. J. Molecular dynamics simulation of discontinuous volume phase transitions in highly-charged crosslinked polyelectrolyte networks with explicit counterions in good solvent. *The Journal of Chemical Physics* **2005**, *123*, 174909.

(41) Mann, B. A.; Holm, C.; Kremer, K. Swelling of Polyelectrolyte Networks. *The Journal of Chemical Physics* **2005**, *122*, 154903.

(42) Quesada-Pérez, M.; Ibarra-Armenta, J. G.; Martín-Molina, A. Computer simulations of thermo-shrinking polyelectrolyte gels. *The Journal of Chemical Physics* **2011**, *135*, 094109.

(43) Mann, B. A.; Lenz, O.; Kremer, K.; Holm, C. Hydrogels in Poor Solvents: A Molecular Dynamics Study. *Macromolecular Theory and Simulations* **2011**, *20*, 721–734, Cover Issue.

(44) Longo, G. S.; de la Cruz, M. O.; Szleifer, I. Molecular Theory of Weak Polyelectrolyte Gels: The Role of pH and Salt Concentration. *Macromolecules* **2011**, *44*, 147–158.

(45) Longo, G. S.; de la Cruz, M. O.; Szleifer, I. Molecular theory of weak polyelectrolyte thin films. *Soft Matter* **2012**, *8*, 1344–1354.

(46) Longo, G. S.; de la Cruz, M. O.; Szleifer, I. pH-Controlled Nanoaggregation in Amphiphilic Polymer Co-networks. *ACS Nano* **2013**, *7*, 2693–2704.

(47) Longo, G. S.; de la Cruz, M. O.; Szleifer, I. Non-monotonic swelling of surface grafted hydrogels induced by pH and/or salt concentration. *The Journal of Chemical Physics* **2014**, *141*, 124909.

(48) Höpfner, J. A new method of seawater desalination via acrylic acid based hydrogels: Synthesis, characterisation, and experimental realisation. Ph.D. thesis, Karlsruher Institut für Technologie (KIT), 2013.

(49) Grest, G. S.; Kremer, K. Molecular dynamics simulation for polymers in the presence of a heat bath. *Physical Review A* **1986**, *33*, 3628–31.

(50) Deserno, M.; Holm, C.; May, S. Fraction of Condensed Counterions around a Charged Rod: Comparison of Poisson-Boltzmann Theory and Computer Simulations. *Macromolecules* **2000**, *33*, 199–206.

(51) Weeks, J. D.; Chandler, D.; Andersen, H. C. Role of Repulsive Forces in Determining the Equilibrium Structure of Simple Liquids. *The Journal of Chemical Physics* **1971**, *54*, 5237.

(52) Kremer, K.; Grest, G. S. Dynamics of entangled linear polymer melts: A molecular-dynamics simulation. *The Journal of Chemical Physics* **1990**, *92*, 5057–5086.

(53) Smith, W. R.; Triska, B. The reaction ensemble method for the computer simulation of chemical and phase equilibria. I. Theory and basic examples. *The Journal of Chemical Physics* **1994**, *100*, 3019–3027.

(54) Weik, F.; Weeber, R.; Szuttor, K.; Breitsprecher, K.; de Graaf, J.; Kuron, M.; Landsgesell, J.; Menke, H.; Sean, D.; Holm, C. ESPResSo 4.0 – an extensible software package for simulating soft matter systems. *European Physical Journal Special Topics* **2019**, *227*, 1789–1816.

(55) Deserno, M.; Holm, C. In *Electrostatic Effects in Soft Matter and Biophysics*; Holm, C., Kékicheff, P., Podgornik, R., Eds.; NATO Science Series II - Mathematics, Physics and Chemistry; Kluwer Academic Publishers: Dordrecht, Nl, 2001; Vol. 46; pp 27–50.

(56) Ninham, B. W.; Parsegian, V. A. Electrostatic potential between surfaces bearing ionizable groups in ionic equilibrium with physiologic saline solution. *Journal of Theoretical Biology* **1971**, *31*, 405–428.

(57) Markovich, T.; Andelman, D.; Podgornik, R. In *Handbook of Lipid Membranes: Molecular, Functional, and Materials Aspects*; Safinya, C. R., Rädler, J., Eds.; Taylor & Francis / CRC Press, 2016; Chapter 1.

(58) Antypov, D.; Holm, C. Optimal cell approach to osmotic properties of finite stiff-chain polyelectrolytes. *Physical Review Letters* **2006**, *96*, 088302.

(59) Jackson, J. D. *Classical Electrodynamics*, 3rd ed.; John Wiley & Sons: New York, 1999.

(60) Staňo, R.; Košovan, P.; Tagliabue, A.; Holm, C. Electrostatically Cross-Linked Reversible Gels—Effects of pH and Ionic Strength. *Macromolecules* **2021**, *54*, 4769–4781.

(61) Tagliabue, A.; Landsgesell, J.; Mella, M.; Holm, C. Can oppositely charged polyelectrolyte stars form a gel? A simulational study. *Soft Matter* **2021**, *17*, 1574–1588.

(62) Landsgesell, J.; Beyer, D.; Hebbeker, P.; Košovan, P.; Holm, C. Electronic Supporting Information and Replication Data for: The pH-dependent Swelling of Weak Polyelectrolyte Hydrogels Modeled at Different Levels of Resolution. https://darus.uni-stuttgart.de/privateurl.xhtml?token=34e36161-a173-46ce-9c7a-82d79ec1606b.

Graphical TOC Entry